J Appl Electrochem (2012) 42:925–934
DOI 10.1007/s10800-012-0478-1

ORIGINAL PAPER

Rhodium electrodeposition on nickel electrodes used for urea electrolysis

Alexander Thomas Miller · Brian Lloyd Hassler · Gerardine G. Botte

Received: 21 May 2012 / Accepted: 21 August 2012 / Published online: 9 September 2012

Abstract A procedure for the constant potential electrodeposition of rhodium onto nickel electrodes, the subsequent surface characterizations, and electrochemical evaluation is presented. The resulting Ni/Rh electrodes were evaluated for their activity as anode catalysts for the electro-oxidation of urea. A detailed procedure for the electrodeposition of Rh onto Ni foil is provided. It is shown that the electrocatalytic performance of Ni/Rh electrodes on the oxidation of urea in alkaline medium is primarily influenced by two electrodeposition parameters: the applied electrodeposition potential and the loading of Rh (mg cm^{-2}). An optimization for electrocatalytic performance based on the electrodeposition potential and Rh loading is demonstrated. The effect of these parameters on visual finish, surface morphology, and crystal structure was also studied.

Keywords Electrodeposition · Urea electrolysis · Hydrogen production · Fuel cells · Wastewater remediation

1 Introduction

A modern trend in wastewater treatment utilizes electrochemical methods to eliminate and/or control chemical pollutants in waste streams [1–7]. Urea, the primary chemical component in urine, is one of the most abundant wastes on the planet. The electrochemical oxidation of urea using a nickel catalyst is currently being investigated for the purpose of not only purifying urea-rich wastewaters, but also producing fuel grade hydrogen [4, 6, 7].

Applications for industrial urea electrolyzers include treatment of farm animal waste, municipal wastewater treatment plants, chemical waste treatment plants, or anywhere significant amounts of urea are concentrated in water. As in the oxidation of many organic compounds at Ni electrodes, the active electrocatalyst is most likely a nickel oxide hydroxide that is continuously reformed from the corresponding reduced nickel hydroxide [7, 8]. Although the precise mechanism for the electro-oxidation of urea is not known, it is thought that oxidation at nickel hydroxide electrodes occurs through indirect, heterogeneous, anodic dehydrogenation [7, 8]. The electrochemical reactions associated with the electrolysis of urea are summarized below [4, 8].

Anode

$$Ni(OH)_2 + OH^- \xrightarrow{Ni} NiOOH + H_2O + e^- \quad (0.49\ V\ vs.\ SHE) \tag{1}$$

$$CO(NH_2)_2 + 6OH^- \xrightarrow{NiOOH} N_2 + 5H_2O + CO_2 + 6e^- \quad (-0.46\ V\ vs.\ SHE) \tag{2}$$

Cathode

$$6H_2O + 6e^- \rightarrow 3H_2 + 6OH^- \quad (-0.83\ V\ vs.\ SHE) \tag{3}$$

Overall

$$CO(NH_2)_2 + H_2O \rightarrow N_2 + 3H_2 + CO_2 \quad (0.37\ V\ total\ cell) \tag{4}$$

Nickel metal has been shown to be the most active electrocatalyst for the oxidation of urea, and it is the low relative cost and abundance of Ni that gives it a significant advantage for use as a catalyst [4–6]. However, the ability

A. T. Miller · B. L. Hassler · G. G. Botte (✉)
Department of Chemical and Biomolecular Engineering,
Center for Electrochemical Engineering Research,
Russ College of Engineering and Technology, Ohio University,
165 Stocker Center, Athens, OH 45701, USA
e-mail: botte@ohio.edu

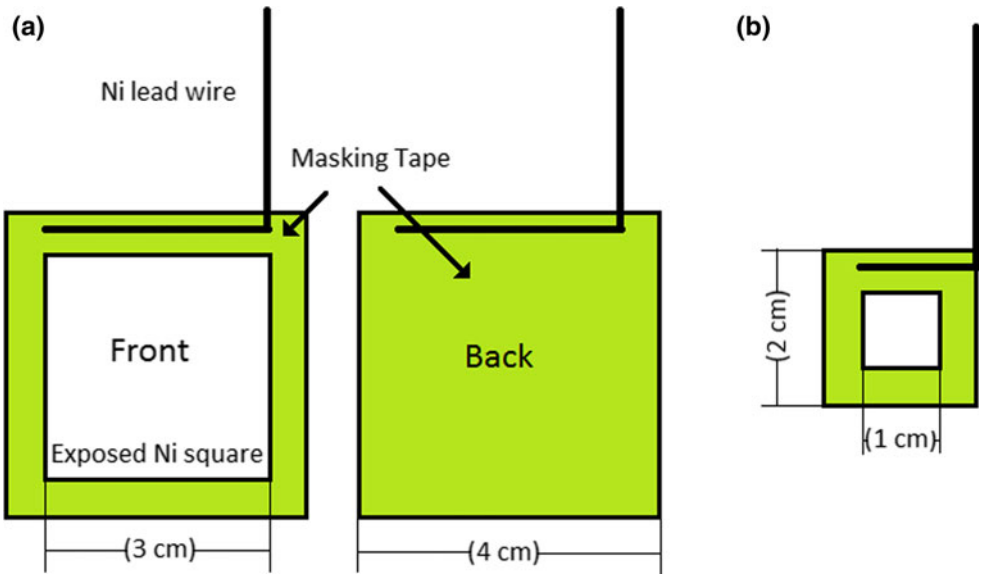

Fig. 1 Model of masked electrodes, **a** masked electrode prior to electrodeposition, **b** quartered electrode used in electrochemical testing. Electrodes were carefully and precisely masked with chemical and temperature-resistant masking tape leaving an exposed area of 9 cm^2 before electrodeposition of Rh. After electrodeposition, electrodes were unmasked and cut into 4 equal squares. 2 out of 4 resulting quartered electrodes were masked again using the same tape for electrochemical tests, while the other 2 were used for SEM and XRD surface characterization

of the electrocatalyst to maintain a high current density is limited due to catalyst deactivation [6]. King and Botte [6] have shown increased catalyst stability and activity of Ni electrodes when a layer of Rh was deposited on the electrode surface and have proposed that a bimetallic Rh–Ni catalyst should be investigated for the purpose of maintaining the catalytic activity of the Ni electrodes.

The modification of Ni catalysts using noble metals has been studied extensively for steam reforming applications where bimetallic catalysts are used to both increase activity and control selectivity [9–11]. It has been shown that the addition of small amounts of Rh to a Ni catalyst increased catalytic activity and stability where emphasis is placed on lower coke-formation rates [10]. Using temperature-programmed desorption (TPD) for CO_2, the authors also show the bimetallic Rh/Ni catalysts' ability to absorb and dissociate greater amounts CO_2 compared to pure Ni catalysts [10]. This is an important finding related to the electrooxidation of urea because the improved performance observed in Ni/Rh catalysts may be related to the desorption of CO_2, which is a product of the oxidation reaction and rate-limiting step of the oxidation of urea as suggested by Daramola et al. [12].

Although future investigations may directly address the CO_2 absorption/desorption characteristics of these electrodes, this study focuses on the procedural preparation, characterization, and analysis of Rh–Ni electrodes with emphasis on the electrodeposition of Rh onto a Ni substrate to be used as a bimetallic anode for the bulk electrolysis of urea. The ability to control loading, morphology, and crystallinity of the resulting Rh–Ni anode catalysts is demonstrated for various electrodeposition conditions, and the performance of the electrodes is then related to these parameters.

2 Experimental methodology

2.1 Electrodeposition techniques

2.1.1 Pretreatments and masking

The substrate material used was an annealed nickel foil purchased from Alfa Aesar (0.005″ thick, 99^+ % Ni on metal basis). Electrodes were cut to 4 × 4 cm squares using a 1.0-mm Ni lead wire spot welded into place. The electrodes were sanded in 2 perpendicular directions with 220 grit sandpaper. After assembly, electrodes were cleaned with acetone and rinsed with deionized water (DI water) before being dried for 10–20 min in an oven at 80 °C. After allowing time to cool, the mass of each electrode was measured in triplicate using an analytical balance accurate to 0.1 mg.

Prior to electrodeposition and after cleaning, electrodes were masked using high temperature polyester tape manufactured by 3 M exposing a 3 × 3 cm square surface on each electrode as shown in Fig. 1a. The electrodes were again rinsed with DI water before being submerged into 1 M H_2SO_4 for 60 s. Performed at room temperature, this acidic descaling pretreatment removes protective oxide films from the Ni surface without significant loss of mass. After the acid dip, the electrodes were quickly rinsed with DI water before being submerged into the plating bath.

In addition to the masking used for electrodeposition, Fig. 1b shows how electrodes were masked for electrochemical testing. It is important to note that electrodes were divided into 2 × 2 cm quarters masked to 1 × 1 cm exposing only Rh/Ni to the electrolysis solutions. Other quarter portions of the cut electrodes were used as

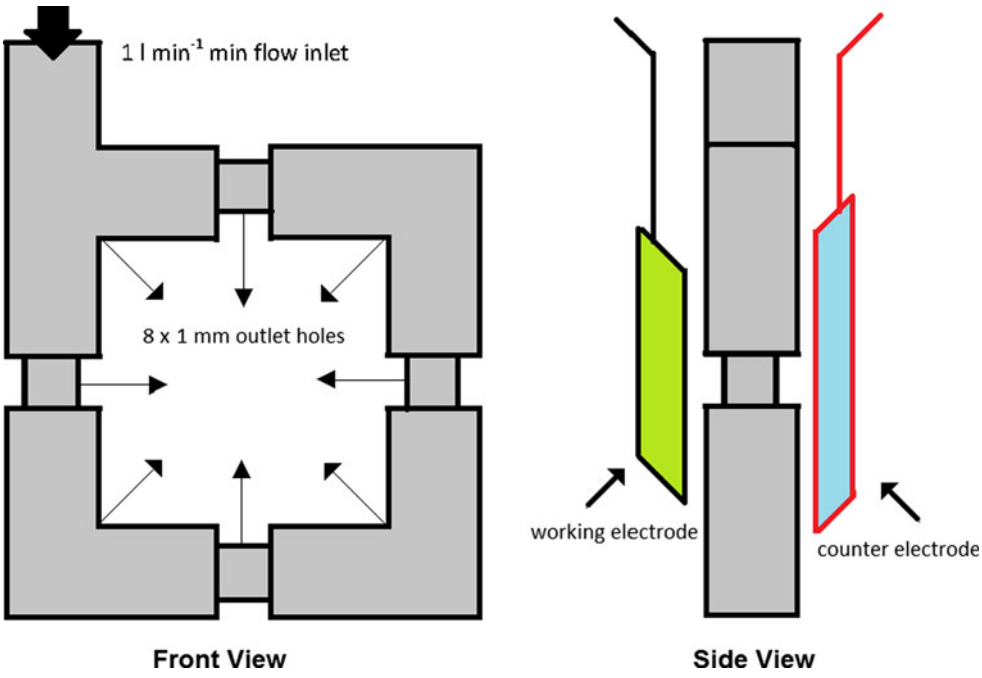

Fig. 2 Front and side view of deposition apparatus. This apparatus, made of standard PVC fittings and nipples, was submerged in a 600-ml Beaker filled with 400 ml of plating solution. A 1 l min^{-1} constant flow rate of plating solution was circulated through the apparatus and the bottom of the beaker for each electrode used. A double junction Ag/AgCl reference electrode was placed at the right edge of the working electrode to monitor potential. This apparatus is limited to solutions that do not interact with PVC

replicates for electrochemical tests and for other evaluation techniques such as scanning electron microscopy (SEM) and X-ray diffraction (XRD).

2.1.2 *Plating procedure*

The plating bath used in this study was composed of 1 M NaCl (ACS grade purchased from Fisher Scientific) with 1.2–1.3 g l^{-1} $RhCl_3(H_2O)_n$ (38.5–45.5 wt% Rh purchased from Alfa Aesar). The concentration of Rh^{3+} ions was maintained between 450 and 500 mg l^{-1} as measured using a Perkin Elmer AAnalyst 400 atomic absorption spectrometer (AAS). AAS techniques showed a mass ratio of approximately 0.38–0.40 g of Rh^{3+} ions per gram of $RhCl_3(H_2O)_n$ salt.

The electrodeposition of Rh onto the prepared Ni electrodes occurred in a 600-ml beaker using 400 ml of solution and a 4-cm magnetic stir bar at 300 rpm. In addition to stir bar agitation, a separate flow apparatus was used to deliver uniform agitation of the plating solution and to hold a constant distance of 2.1 cm between the working and counter electrodes (5 × 5 cm Pt foil). The 4 N purity Pt Foil (thickness 0.004″) was purchased from ESPI metals. The flow apparatus, shown in Fig. 2, was made using ½ inch schedule 80 PVC pipe fittings and nipples purchased from McMaster Carr. Eight 1-mm holes were drilled at the center point of all fitting corners and nipples. During electrodeposition, a Cole-Parmer model 75211-10 gear pump was used to maintain a constant circulation flow rate of 1 l min^{-1}. Flow rates were measured with a Blue-White industries Ltd. Model F-400 tube rotameter.

The deposition potentials for each electrode were applied with a Solartron model 1470E Potentiostat. A Ag/AgCl reference electrode was used with a luggin capillary filled with 1 M NaCl to control the deposition half potential. Electrodeposition of Rh onto the electrodes using constant potential techniques was terminated at the desired charge for each electrode. The charge, Q, is directly proportional to the mass, w, of the resulting deposit defined by the following equation derived from Faraday's law [13]

$$w = \frac{A_{wt} Q \, CE}{nF} \tag{5}$$

where A_{wt} is the atomic weight of the involved species, n is the number of electrons, F is Faraday's constant, and CE is the fractional charge efficiency of the electrochemical reaction.

2.2 Electrode evaluation

2.2.1 *Cyclic voltammograms*

Electrochemical experiments were performed using the same Solartron model 1470E Potentiostat. Solutions were prepared using certified ACS grade urea and NF/FCC pellets of 10–15 % H_2O purchased from Fisher Scientific. Sample electrodes were first cut into quarters (2 × 2 cm squares) and masked after Rh electrodeposition as previously described. For all cyclic voltammetry (CV) experiments, electrodes were first evaluated inside a background 5 M KOH solution, then a 5 M KOH + 0.33 M urea solution immediately after.

In each CV experiment, working electrodes were placed opposite a 5 × 5 cm Pt foil counter electrode for 10 cycles allowing the CV profiles to reach a sustained periodic state. A 2-cm separation between the working and counter electrodes was maintained. The half-cell potential for each sample electrode was monitored using a Hg/HgO reference electrode inside a luggin capillary with 5 M KOH. Beginning at 0.0 V versus Hg/HgO, the potential was cycled between 0.0 and 0.7 V versus Hg/HgO at a scan rate of 20 mV s^{-1}.

2.2.2 *Surface characterization*

Scanning electron microscopy (SEM) images were taken using a JEOL JSM-6390 scanning electron microscope at 15 kV. XRD analyses were performed on a Rigaku Ultima IV X-ray diffractometer using a Cu Kα radiation source ($\lambda = 1.5401$ Å). The source operated at 40 kV and 100 mA. The 2θ angular region between 30° and 100° was explored at a 0.5° s^{-1} scan rate. The average particle size and lattice parameter for the Ni and Ni/Rh crystallites were calculated using the full width at half maximum (FWHM) and angular position (2θ max) of the Ni (1 1 1) diffraction peak and fit using the Gaussian function.

3 Results/discussion

3.1 Interpretation of cyclic voltammograms

Potential sweep methods such as CVs are primarily useful for their qualitative diagnostic strengths. In this case, where a complex electrochemical system is being studied and where a precise mechanism is not known, the results from both test solutions can be considered semi-quantitative [14]. Figure 3 shows a typical CV curve in 5 M KOH and 5 M KOH + 0.33 M urea solutions for two separate Rh/Ni electrodes of different Rh loadings, as well as an unmodified Ni electrode. The fact that all electrodes in this study behave similarly in their respective *i–E* profiles should not be understated (where *i* is the current density in A cm^{-2} and *E* is the potential of the electrode in V vs. Hg/HgO).

For Rh-modified electrodes in the 5 M KOH CV, an oxidation peak is observed in the forward scan that is associated with the oxidation of $Ni(OH)_2$ to NiOOH and is located at 0.414 ± 0.004 V versus Hg/HgO with uncertainty based on the standard deviation of electrodes tested. However, this is not the case with unmodified Ni foil electrodes where oxidation peaks were observed at 0.442 ± 0.006 V versus Hg/HgO. A reduction peak associated with the reduction of NiOOH to $Ni(OH)_2$ was also observed on the reverse scan for Rh/Ni electrodes and unmodified Ni electrodes at 0.334 ± 0.016 V versus Hg/HgO and 0.370 ± 0.011 V versus Hg/HgO, respectively. For Rh/Ni electrodes, the redox potentials are consistent with literature values for the so-called α-$Ni(OH)_2$/γ-NiOOH redox couple, where α and γ denote a general subset of hydrated and disordered crystal structures [15, 16]. Conversely, the redox potentials observed for unmodified Ni electrodes were more consistent with the β-$Ni(OH)_2$/β-NiOOH redox couple, where the β crystal structures are

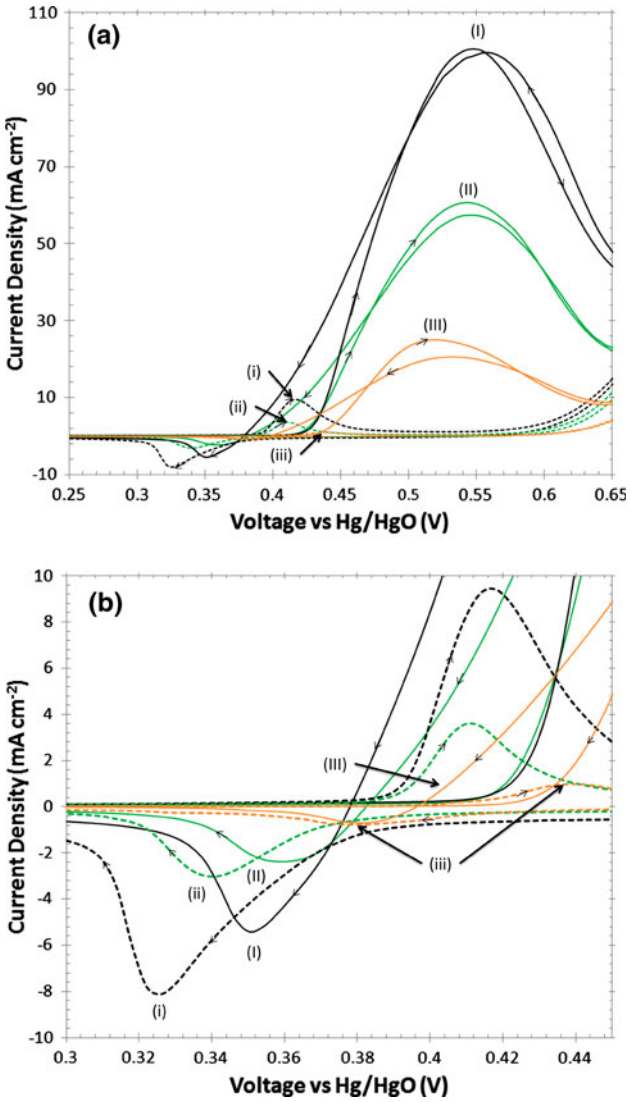

Fig. 3 Typical cyclic voltammogram for modified and unmodified Rh/Ni electrodes in 5 M KOH (*i dashed lines*) and 5 M KOH + 0.33 M urea (*I solid lines*) solutions at a scan rate of 20 mV s^{-1}. **a** Oxidation peaks in detail. **b** Reduction peaks in detail. *I* and *i* data, −0.71 mg cm^{-2} Rh deposited at −0.4 V versus Ag/AgCl. *II* and *ii* data, −0.21 mg cm^{-2} Rh deposited at −0.4 V versus Ag/AgCl. *III* and *iii* data, unmodified Ni electrode. Reduction peak current densities for electrodes in 5 M KOH are greater than peak current densities for the same electrode in 5 M KOH + 0.33 M urea, suggesting an indirect chemical reaction reduces NiOOH and oxidizes urea prior to the electrochemical reduction of NiOOH to $Ni(OH)_2$. This also helps to explain the presence of an oxidation peak during the reverse scan

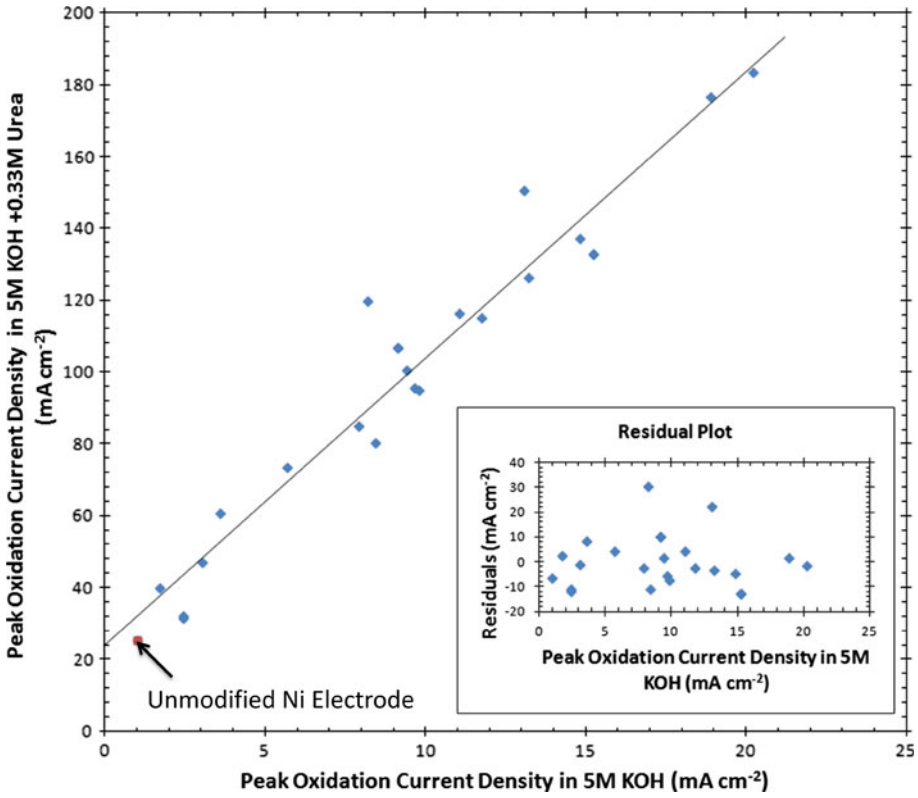

Fig. 4 Proportional relationship between Rh/Ni electrodes' CV peak current density in 5 M KOH and the CV peak current density in 5 M KOH + 0.33 M Urea at a scan rate of 20 mV s^{-1}. The CV peak current density in 5 M KOH is associated with the oxidation of $Ni(OH)_2$ to NiOOH. This relationship suggests that the activity of Rh-modified Ni electrodes for the electrolysis of urea is directly proportional to the amount of NiOOH able to be formed on the surface as measured by the CV peak current density in 5 M KOH. An unmodified Ni electrode was the worst performing electrode and is marked. The Rh-modified Ni electrodes do not progress linearly due to loading

more ordered and less hydrated [15]. It is important to note that these redox couples occur only when Ni is present, and that a pure Rh electrode without Ni will not show a redox couple in this region [6].

When a urea solution is used, the behavior of the electrodes is not as well defined by the literature. The peak oxidation current for the CV using 5 M KOH + 0.33 M urea solution occurs on both the forward and reverse scans at a larger range of potentials between 0.55 and 0.65 V versus Hg/HgO with an average forward potential of 0.574 ± 0.042 V versus Hg/HgO, which is on average 0.161 V more positive than in the absence of urea. A reduction peak also occurs on the reverse scan of the 5 M KOH + 0.33 M urea CV at a potential of 0.356 ± 0.016 V versus Hg/HgO, which is on average 0.022 V more positive than the observed peak in 5 M KOH. A paired two-tailed *t* test between the mean reduction peak potentials of electrodes in 5 M KOH and the same electrodes in 5 M KOH + 0.33 M urea reveals a probability of 0.11 % that the potentials are not significantly different. This implies that the addition of urea to the KOH electrolyte slightly increases the peak reduction potential relative to a Hg/HgO reference electrode, and could be shifting the surface structure of Rh-modified Ni electrodes from α to β.

In addition to the difference in reduction potentials, there are also differences in the relative reduction peak magnitudes between the 5 M KOH and 5 M KOH + 0.33 M urea solutions. The reduction peak current density is always slightly less in the presence of urea as observed in Fig. 3. This supports the hypothesis of urea being oxidized indirectly at the anode because NiOOH would be consumed by the indirect chemical reaction with urea, and due to the lower availability of NiOOH on the reverse scan the reduction peak of NiOOH to $Ni(OH)_2$ is relatively smaller. This hypothesis is supported by a mechanism reported by Vedharathinam and Botte [7] and similar indirect oxidation mechanisms at $Ni(OH)_2$ electrodes for methanol [17] and aspirin [18]. However, some reservations do still exist on the validity of this mechanism [7].

For all 24 electrodes tested, there was a strong correlation between the NiOOH peak in the 5 M KOH solutions and the forward scan peak oxidation current density of the 5 M KOH + 0.33 M urea solutions. Figure 4 shows this strong proportional link for a number of Rh/Ni electrodes. An unmodified Ni electrode is the lowest performing electrode shown in the plot, while all other points represent different Rh-modified Ni electrodes. It is important to note that without exception, the addition of Rh improves electrode performance. However, oxidation currents are not directly related to Rh loading, but are instead related to both the loading and the morphology of the deposit, which will be discussed in the following sections.

A linear regression was performed using the peak oxidation current densities of electrodes in 5 M KOH (associated with the oxidation of $Ni(OH)_2$ to NiOOH) to predict the peak

oxidation current density for electrodes in 5 M KOH + 0.33 M urea. This resulted in a simple linear equation with a slope of 7.99 ± 0.42 (mA in 5 M KOH + 0.33 M Urea per mA in 5 M KOH), an intercept of 24 ± 5 mA, and an R^2 value of 0.941 with coefficient uncertainties based on the standard error. Analysis of variance (ANOVA) performed on the regression produced an F value of 353. The *F* significance relating the probability of a random 24 point dataset resulting in an equivalent model is 4.76×10^{-15}, meaning it is extremely unlikely that the relationship between the two peaks is due to random chance. A residual plot of the involved points, at the lower right corner of Fig. 4, shows residuals randomly spaced around zero further solidifying the proportional relationship.

The proportional relationship between the NiOOH peak current density in the 5 M KOH solutions and the forward scan peak current density of the 5 M KOH + 0.33 M solutions suggests that the amount of NiOOH formed on a Ni or Ni/Rh electrode is related to the amount of urea that is oxidized during urea electrolysis. It is likely that the deposited Rh promotes the Ni electrodes by allowing a greater proportion of NiOOH to exist at the potential range selected.

3.2 The effect of electrodeposition potential

3.2.1 Electrodeposition efficiency

The effect of voltage on Faraday charge efficiency was studied for the previously described electrodeposition/agitation setup. Electrodes were prepared at a range of voltages from −0.35 to −0.75 V versus Ag/AgCl. All electrodes were immediately removed from the deposition bath after 15.8 °C was discharged. Using Eq. (5), this charge corresponds to a loading of 5.625 mg Rh (0.625 mg cm^{-2} for a 9 cm^2 electrode) at 100 % Faraday efficiency based on the total current passed. Observed differences in electrodeposition efficiency are shown in Fig. 5.

Actual efficiencies were determined using Eq. (5), where the measured amount of Rh deposited was compared to the theoretic value. The amount of Rh deposited was defined as the difference between the dry mass of the electrode before and after electrodeposition. Figure 5 shows the relationship between the applied half-cell potential and current efficiency. Error bars were based on the standard deviation of 3 replicate electrodes plated at −0.55 and −0.60 V versus Ag/AgCl. It is important to note the decrease of efficiency of the plating bath at lower applied potentials and the development of a chlorine smell of a used plating bath. This decrease in efficiency at lower potentials is due to a parasitic reaction of Cl^- reducing to Cl_2 gas in place of reducing Rh^{+3} ions. All solutions used in these experiments were fresh and replaced after every 2 electrodes plated.

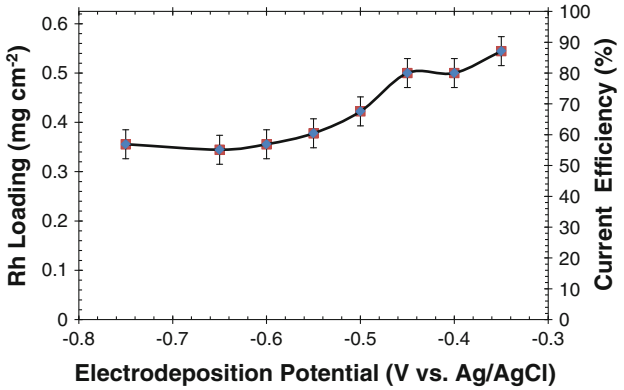

Fig. 5 The effect of electrodeposition potential on electrodeposition current efficiency in a 1.24 mg l^{-1} $RhCl_3$ + 1.0 M NaCl plating bath at room temperature. Rh was deposited on the electrodes in this figure at each specified potential until a total charge of 15.8 C was passed. At 100 % efficiency, this charge corresponds to 5.625 mg of Rh, or 0.625 mg cm^{-2} for a 9 cm^2 electrode. This figure can be used as a rough guide for estimating electrodeposition efficiency of Rh onto Ni in similar systems

3.2.2 Morphology

The effect of electrodeposition potential on the visual finish of Ni–Rh electrodes was apparent upon visual observation of the electrodes. As deposition potential increases from −0.35 to −0.75 V versus Ag/AgCl, the deposit changes from a light silvery gray (87.1 % current efficiency, Fig. 5) to a dark dull powdery black (56.9 % current efficiency, Fig. 5).

Figure 6 shows SEM images of sample electrodes prior to electrochemical testing for a range of deposition potentials. In all images, the light gray and brightest portions are representative of a layer of Rh with the darker portions between nodules and cracks being the Ni substrate backing. In all cases, nodules appear to have been formed along perpendicular groves created by the sanding pretreatment, although this is most evident at higher voltages. The deposit mechanism of growth for electrodes plated in this study is one likely dominated by nucleation coalescence rather than layer growth [13].

In Fig. 6a, an image of an electrode plated at −0.35 V versus Ag/AgCl has relatively large nodules (1–2 μm) coalesced in a thick well-defined layer. The cracks and pealing of this layer suggest that it was not well adherent to the Ni substrate. In Fig. 6b, an image of an electrode plated at −0.45 V versus Ag/AgCl shows smaller nodules (0.5–1.5 μm) that are less coalesced on the surface of a layer of Rh. This suggests that when the Rh deposit was growing, a layer of smaller nucleation sites competed for Rh ions before coalescence. After coalescing, the larger of the competing nodules continued to grow, creating the morphology observed. In Fig. 6c, an image of an electrode plated at

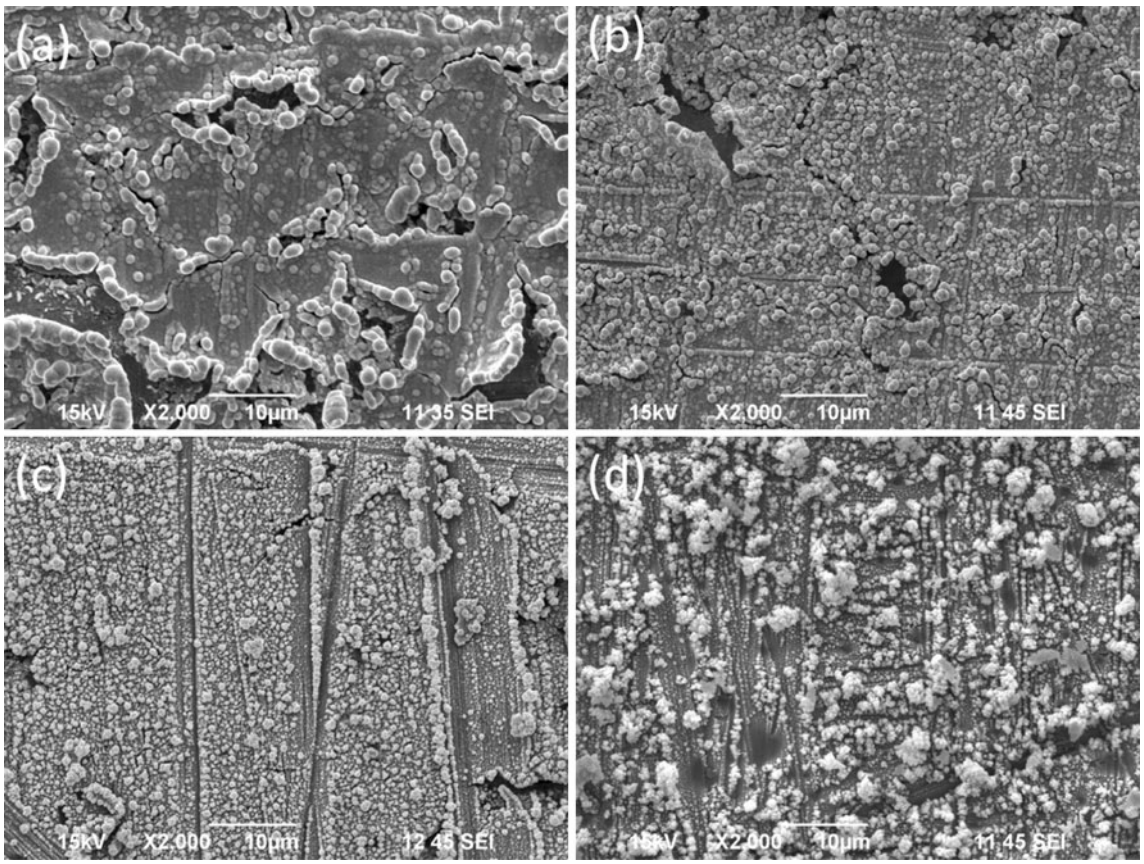

Fig. 6 The effect of electrodeposition potential on morphology. SEM images at plating potentials **a–d** −0.35, −0.45, −0.55, and −0.75 V versus Ag/AgCl. In Fig. 6a, an image of an electrode plated at −0.35 V versus Ag/AgCl has relatively large nodules (1–2 μm) coalesced in a thick well-defined layer. In Fig. 6b, an image of an electrode plated at −0.45 V versus Ag/AgCl shows smaller nodules (0.5–1.5 μm) that are less coalesced on the surface of a layer of Rh. In Fig. 6c, an image of an electrode plated at −0.55 V versus Ag/AgCl shows a more extreme range of node sizes (<0.5–1 μm). In Fig. 6d, an image of an electrode plated at −0.75 V versus Ag/AgCl shows an instance where small nodes (<0.5 μm) coexist with large feathery dendrites (2–3 μm)

−0.55 V versus Ag/AgCl shows a more extreme range of node sizes (<0.5–1 μm). In this case, nodes do not coalesce in the same-layered fashion. Instead the darker Ni substrate is visible around isolated nodes. The only instances of coalescence occur along the ridges of the sanded Ni substrate. In Fig. 6d, an image of an electrode plated at −0.75 V versus Ag/AgCl shows an instance where small nodes (<0.5 μm) coexist with large feathery dendrites (2–3 μm). It is important to note the voids of similar size and shape as the dendrites where the darker Ni substrate is visible without nodules of any type. It is very likely that these voids were the result of dendrites falling off. In the case of this electrode and with other electrodes plated above −0.65 V versus Ag/AgCl, the coating was very dark and powdery.

3.2.3 Activity as a urea electrocatalyst CV

Electrodes with the same approximate Rh loading ($\sim$0.36 mg cm^{-2}) were selected for electrochemical evaluation using the described CV techniques. These Rh/Ni electrodes were compared using the forward scan peak current density in 5 M KOH + 0.33 M urea. Figure 7 shows the dependency of the peak current density on the electrodeposition plating potential. Error bars in the figure are based on the standard deviation of the same replicate samples used in Fig. 5. The optimal electrodeposition voltage (highest peak current density) for this particular Rh loading is −0.60 V versus Ag/AgCl.

3.3 The effect of Rh loading: activity as a urea electrocatalyst

To study the effect of Rh loading on electrode performance, electrodes were plated at two separate voltages and several Rh loadings. Loadings for each electrode were controlled by tracking the charge of the electrode throughout electrodeposition and terminating at the desired charge. Charge efficiencies for this set of electrodes were calculated based on electrodeposition potential using Fig. 5.

Figure 8 illustrates the performance differences of electrodes plated at −0.4 and −0.6 V versus Ag/AgCl at various loadings. Average peak current densities from urea

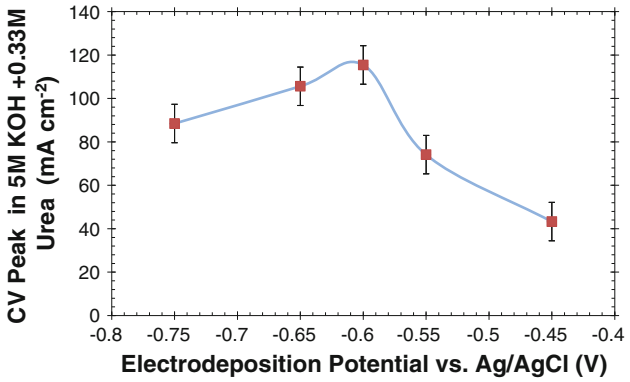

Fig. 7 Effect of electrodeposition potential on electrode performance at a constant loading of 0.36 mg cm^{-2}. This figure shows a maximum activity when electrodes were deposited at −0.60 V versus Ag/AgCl. Error bars for this figure were determined by the average standard deviation of 3 replicate electrodes plated at −0.55 and −0.60 V versus Ag/AgCl

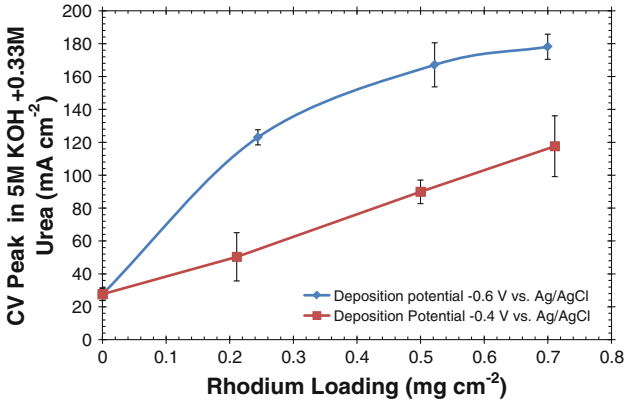

Fig. 8 Effect of Rh loading on electrode performance. *Diamond markers* denote electrodes plated at −0.6 V versus Ag/AgCl, while *square markers* denote electrodes plated at −0.4 V versus Ag/AgCl. Electrodes plated at 0.6 V versus Ag/AgCl appear to approach a maximum level of performance with increased Rh loading, while electrodes plated at −0.4 V versus Ag/AgCl appear to increase linearly

CVs were plotted from 2 to 3 replicates at each loading with the standard deviations of these replicates used as the error bars for each point. Performance increases with Rh loading for each deposition potential; however, it increases slower and more linearly with electrodes with Rh deposited at −0.4 V versus Ag/AgCl. Electrodes where Rh was deposited at −0.6 V versus Ag/AgCl were able to produce much higher current densities, but instead of increasing linearly over the range tested, the trend appears to approach a maximum. At equivalent loadings, the performance differences between electrodes deposited at −0.4 and −0.6 V versus Ag/AgCl are due to differences in morphology.

3.4 The effect of Rh loading and deposition potential: XRD analysis

Figures 9 and 10 show the XRD pattern for the Rh-modified Ni electrodes of various loadings formed at −0.6 and −0.4 V versus Ag/AgCl. Figure 9a, curve iv, shows the XRD patterns for the modified Ni electrodes; the characteristic peaks of a crystalline face-centered cubic (fcc) Ni phase from the (1 1 1), (2 0 0), (2 2 0), (3 1 1), and (2 2 2) planes were observed at approximately 44.49°, 51.85°, 76.38°, 92.93°, and 98.44°, respectively. Upon the deposition of Rh, the typical fcc Ni (1 1 1) diffraction peak broadens (Fig. 9b), indicating the presence Ni–Rh interactions. Despite the peak broadening, the absence of a shift in Ni (1 1 1) diffraction pattern indicates that no Ni/Rh alloys are present on the Ni surface [19]. The appearance of peaks at 41.07°, 47.79°, 69.90°, 84.40°, and 89.11° are associated with Rh (1 1 1), (2 0 0), (2 2 0), (3 1 1), and (2 2 2), respectively. The presence of peaks associated Rh and no shift in the Ni (1 1 1) diffraction pattern indicates that Rh is present in the monometallic form. The Ni (1 1 1) crystal phase lattice parameter (3.525 A) Rh/Ni bimetallic is consistent with the lattice parameter of the unmodified nickel (3.524 A), confirming that nickel and rhodium are present in independent monometallic phases.

However, upon the deposition of Rh onto Ni at an applied potential −0.4 V versus Ag/AgCl (Fig. 10), the Ni (1 1 1) peak transitions from 44.41° to 44.46°, 44.56°, and 44.60°, for loadings of 0.21, 0.50, and 0.71 mg cm^{-2} Rh, respectively. The shift in the Ni (1 1 1) peak indicates alloy formation. However, the presence of constant Rh (1 1 1) peaks suggests that not all the Rh is incorporated into the bulk Ni phase. The lattice parameters for the Ni/Rh electrodes decrease from the bulk Ni value (3.525 A) to values of $a = 3.517$, 3.501, and 3.495 A for loadings of 0.21, 0.50, and 0.71 mg cm^{-2} Rh, respectively. The decrease in the observed lattice parameter with Rh is consistent with the fabrication of Rh/Ni catalysts on Al_2O_3 [19]. The shift in the Ni (1 1 1) peak and changes in the lattice parameter indicate that the system is an alloy rather than the mixture of monometallic or core–shell nanoparticles. These results indicate that an applied potential is a critical parameter in electrodeposition of Rh on Ni substrates. The alloy formation described above is consistent with either sequential ion implantation [20] or structural rearrangement of the metal phases at different applied potentials [21].

4 Conclusions

Rh/Ni electrodes were prepared using Ni foil substrates and electrodepositing Rh using constant potential techniques. It was found that the deposition potential had a significant effect on electrodeposition current efficiency (Faraday efficiency), visual finish, and the morphology of the deposit. In general, the current efficiency (of the

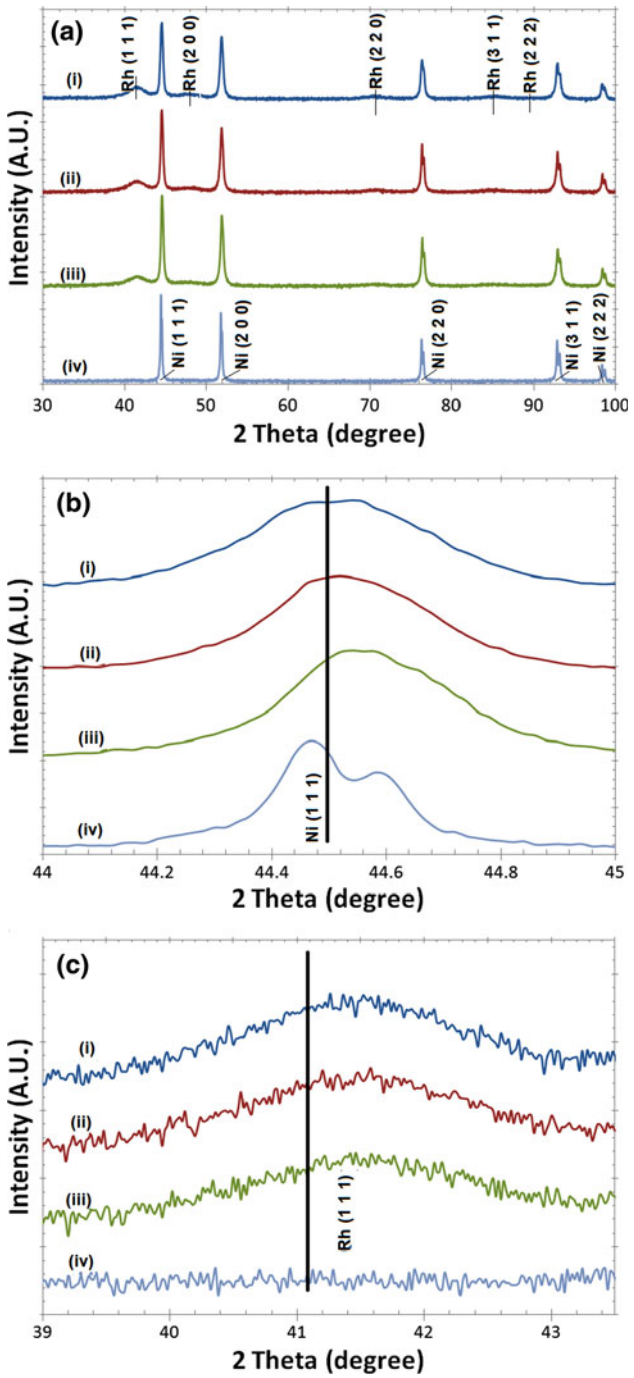

Fig. 9 XRD pattern for electrodes plated at −0.6 V versus Ag/AgCl. **a** full spectrum, **b** Ni (111), **c** Rh (111); with various loadings *i–iv* 0.70, 0.52, 0.24, and 0.00 mg cm^{-2}

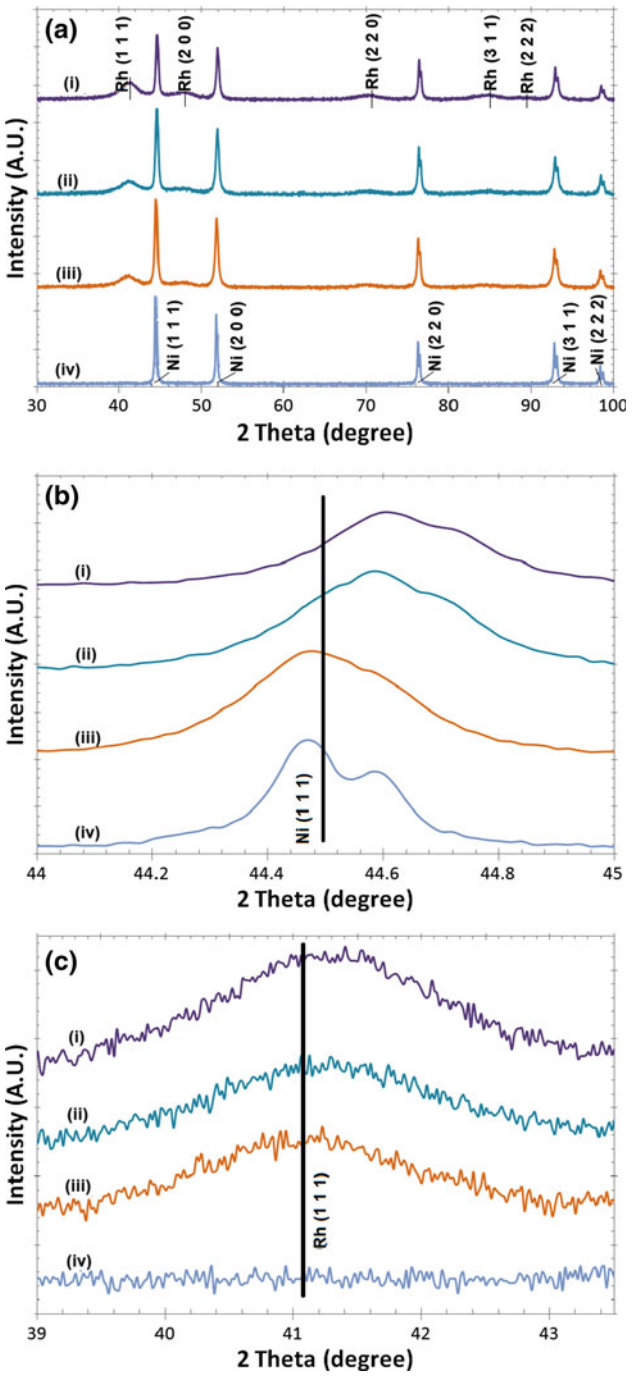

Fig. 10 XRD pattern for electrodes plated at −0.4 V versus Ag/AgCl. **a** Full spectrum, **b** Ni (111), **c** Rh (111); with various loadings *i–iv* 0.71, 0.50, 0.21, and 0.00 mg cm^{-2}

electrodeposition) decreases with more negative electrodeposition potentials. When Rh is deposited on Ni at lower potentials (−0.35 to −0.45 V vs. Ag/AgCl), electrodes are a light silvery gray with a surface morphology of large coalesced nodules. At more negative voltages, −0.45 to −0.55 V versus Ag/AgCl, the deposited Rh becomes a darker gray with morphology of smaller, less coalesced nodules. At the most negative deposition potentials used in this study, −0.55 to −0.75 V versus Ag/AgCl, electrodes are dark black and powdery. The morphology of Rh/Ni electrodes plated at these voltages is characterized by non-coalesced small nodules of Rh with large Rh dendrites.

Experimental results using Rh/Ni electrodes show a direct correlation between the peak current density in 5 M

KOH and the peak current density achieved during the CV in 5 M KOH + 0.33 M urea. This implies a direct relationship between the amount of NiOOH on the electrode surface and the performance of an electrode during urea electro-oxidation. It was found that the addition of Rh increases the current density of electrodes in all CVs performed; and, because of this and the above relationship, it is suggested that one role of Rh in a Rh/Ni electrode used for urea electrolysis is to facilitate the oxidation of $Ni(OH)_2$ to NiOOH, which is the active catalyst in the oxidation of urea. This is in addition to the increase in electrode stability as observed by King and Botte [6].

XRD analyses of the Ni–Rh electrodes show a difference in the alloy characteristics of Ni and Rh at the surface of the electrodes when plating at −0.4 and −0.6 V versus Ag/AgCl. It was found that when Rh is deposited onto Ni at lower voltages, a higher degree of Ni–Rh alloying takes place than at higher voltages. It was shown that the best catalytic performance takes place when monometallic crystallites of Rh are deposited onto a Ni surface instead of an alloy of Ni and Rh. These results support a hypothesis where a surface of pure, polycrystalline Ni in conjunction with pure, polycrystalline Rh is able to support a higher proportion of the active species, NiOOH, than compared to an alloyed Ni/Rh electrode as demonstrated on a macroscopic level by King and Botte [6].

The initial performance tests of the described Rh/Ni electrodes suggest an optimum plating voltage of −0.60 V versus Ag/AgCl at a Rh loading of 0.5 mg cm^{-2}. However, these results are based on initial short-term performance and should not be misconstrued. Although initial performance may be higher, long-term testing may reveal instability in electrodes with fragile Rh dendrites.

Acknowledgments The authors are thankful for the financial support from the Center for Electrochemical Engineering Research at Ohio University and the Department of Defense through the U.S. Army Construction Engineering Research Laboratory (W9132T-09-1-0001). The content of the work does not reflect the position or the policy of the U.S. government.

References

1. Yan W, Wang D, Botte GG (2011) Nickel and cobalt bimetallic hydroxide catalysts for urea electro-oxidation. Electrochim Acta 61:25–30
2. Simka W, Piotrowski J, Robak A, Nawrat G (2009) Electrochemical treatment of aqueous solutions containing urea. J Appl Electrochem 39:1137–1143
3. Jara CC, Di Giulio S, Fino D, Spinelli P (2008) Combined direct and indirect electroxidation of urea containing water. J Appl Electrochem 38:915–922
4. Boggs BK, King RL, Botte GG (2009) Urea electrolysis: direct hydrogen production from urine. Chem Commun 4859–4861
5. King RL, Botte GG (2011) Hydrogen production via urea electrolysis using a gel electrolyte. J Power Sources 196:2773–2778
6. King RL, Botte GG (2011) Investigation of multi-metal catalysts for stable hydrogen production via urea electrolysis. J Power Sources 196:9579–9584
7. Vedharathinam V, Botte GG (2012) Understanding the electrocatalytic oxidation mechanism of urea on nickel electrodes in alkaline medium. Electrochimica Acta
8. Schafer HJ (1987) Oxidation of organic-compounds at the nickel-hydroxide electrode. Top Curr Chem 142:101–129
9. Tomishige K (2007) Oxidative steam reforming of methane over Ni catalysts modified with noble metals. J Jpn Petrol Inst 50: 287–298
10. Hou ZY, Yashima T (2003) Small amounts of Rh-promoted Ni catalysts for methane reforming with CO2. Catal Lett 89:193–197
11. Wang LS, Murata K, Inaba M (2005) Steam reforming of gasoline promoted by partial oxidation reaction on novel bimetallic Ni-based catalysts to generate hydrogen for fuel cell-powered automobile applications. J Power Sources 145:707–711
12. Daramola DA, Singh D, Botte GG (2010) Dissociation rates of urea in the presence of NiOOH catalyst: a DFT analysis. J Phys Chem A 114:11513–11521
13. Schlesinger M, Paunovic M (2000) Modern electroplating, vol xiv. Wiley, New York, p 868
14. Bard AJ, Faulkner LR (2001) Electrochemical methods: fundamentals and applications, vol xxi. Wiley, New York, p 833
15. Oliva P, Leonardi J, Laurent JF, Delmas C, Braconnier JJ et al (1982) Review of the structure and the electrochemistry of nickel hydroxides and oxy-hydroxides. J Power Sources 8:229–255
16. Barnard R, Randell CF, Tye FL (1980) Studies concerning charged nickel hydroxide electrodes I. Measurement of reversible potentials. J Appl Electrochem 10:109–125
17. Danaee I, Jafarian M, Forouzandeh F, Gobal F, Mahjani MG (2008) Electrocatalytic oxidation of methanol on Ni and Ni–Cu alloy modified glassy carbon electrode. Int J Hydrog Energy 33:4367–4376
18. Majdi S, Jabbari A, Heli H (2007) A study of the electrocatalytic oxidation of aspirin on a nickel hydroxide-modified nickel electrode. J Solid State Electrochem 11:601–607
19. Lakhapatri SL, Abraham MA (2009) Deactivation due to sulfur poisoning and carbon deposition on Rh–Ni/Al_2O_3 catalyst during steam reforming of sulfur-doped *n*-hexadecane. Appl Catal A 364:113–121
20. Magruder RH, Wittig JE, Zuhr RA (1993) Wavelength tunability of the surface-plasmon resonance of nanosize metal colloids in glass. J Non-Cryst Solids 163:162–168
21. Bond AM, Fletcher S, Marken F, Shaw SJ, Symons PG (1996) Electrochemical and X-ray diffraction study of the redox cycling of nanocrystals of 7,7,8,8-tetracyanoquinodimethane—observation of a solid–solid phase transformation controlled by nucleation and growth. J Chem Soc-Faraday Trans 92:3925–3933